Corium Interface Flow Dynamics Investigation During Severe Accident in Pressurised Water Reactors Using Compressive Advection Interface Capturing Method

Stephen A. Ajah,[1,2] Lateef Akanji,[3] and Jefferson Gomes[1]
[1)] *Fluid Mechanics Research Group, School of Engineering, University of Aberdeen, UK, AB24 3UE*
[2)] *Applied Renewable & Sustainable Energy Research Group, Department of Mechanical Engineering, University of Nigeria, Nsukka, Nigeria, P.M.B 1042*
[3)] *Chemical Processes and Materials Research Group, School of Engineering, University of Aberdeen, UK, AB24 3UE*

(*Electronic mail: s.ajah.21@abdn.ac.uk.)

Past nuclear accident occurrences raised strong concerns which led to research on nuclear safety. One of the major causes of nuclear accidents is the impeded circulation of core coolant, leading to decay heat removal cessation, and rapid temperature rise. If uncontrolled, this results in critical heat flux (CHF), loss of coolant accidents (LOCA) and core dryout. Detailed melted core relocation (i.e., nuclear fuel, graphite, and zircaloy) need to be investigated through interface capture and multimaterial flow model coupling, which have not been done in previous studies. This work aims to investigate the impacts of temperature and core material composition on the flow dynamics during core relocation. In this study, mass fraction is discretised using a streamlined upwind Petrov-Galerkin (SUPG) method spatially and a modified Crank-Nicolson method temporally to accurately capture fluid interfaces using a high-order accurate flux-limiter. Two core material composition cases (individual material properties case and bulk material properties case) were considered to assess the impact of temperature and core materials composition on both flow dynamics and computational time. Temperature has a significant impact on core material transport and corium flow dynamics during core relocation. Bulk materials properties case has greater impact of temperature on its corium resulting in faster materials transport, but with higher computation time.

I. Introduction

One strategy to address the global energy crisis is through nuclear power, despite the fact that its high heat output during operation makes it susceptible to catastrophic harm. In light of nuclear reactor accidents at Fukushima, Chernobyl, Three Mile Island, and other locations, risk and safety studies are vital to understand the origins and progression of such accidents[1,2]. In nuclear water reactors, fuel rods contain nuclear material (i.e., enriched uranium fuel), which undergo fission reactions with release of heat. Cooling systems (with water as a coolant) extract this heat and maintain reactors at safe temperature. In pressurised water reactors (PWRs), if there is a loss of coolant due to a failure in the cooling system, the heat generated by the ongoing nuclear reactions may cause a significant rise in the temperature of the reactor core. This might result in core dryout, loss-of-coolant accidents (LOCA), and critical heat flux (CHF) within the coolant channel if not appropriately managed at an early stage[3].

Core materials, including fuel rods and structural components, are subjected to extreme thermal stress conditions. This results in changes of thermophysical properties, such as thermal conductivity, specific heat, and mechanical strength, leading to phase transitions, including melting. Molten fuel and cladding form the corium (a mixture of melted fuel, cladding, and reactor coolant), which being highly radioactive, can potentially breach the containment vessel. Core relocation occurs as a result of the interaction between corium and structural materials, which compromises the integrity of the reactor containment.

Fuel rods overheat during CHF events, triggering LOCA, which is associated with a sharp reduction in local heat flux as a result of nucleation boiling. Common features of LOCA include rapid system pressure drop, abrupt local heat flux reduction, core dryout, cladding and fuel rod ballooning, core relocation, high temperature steam oxidation, hydrogen release, and core degradation[3–5]. LOCA leads to reduced reactor's cooling capacity with large heat accumulation, resulting in local hydrodynamic instabilities[6,7]. In assessing CHF, post-CHF, LOCA events and core relocation, multiphase interface-capturing modelling of the reactor core may help predict flow dynamics in the reactor core. Modelling the behaviour of the material interface during severe accidents is essential for fundamental understanding of material interactions and system flow dynamics[8,9].

In order to present an adequate analysis of the multiphase flow dynamics during core relocation events, it is crucial to track the interfaces between different materials (i.e., melted nuclear fuel and cladding). Interface modelling primarily employs two methods: Eulerian and Lagrangian tracking techniques. The element (mesh cell) carrying discretised quantities is transported over the continuous media in Lagrangian schemes, whereas the grid is fixed in the Eulerian approach, while the fluid moves between computational cells[10]. Numerous fluid dynamics and transport problems have been solved using interface tracking and capturing techniques[11–14]. Some of the main types of interface capture techniques are volume of fluid (VOF), level set (LS), and phase field methods. Among these, VOF is the most efficient and reliable approach due to its mass conservation ability across the interfaces[14]. Using an implicit technique to adjust mesh refinement during calculations with accurate mass conservation, VOF methods create moving contact lines along no-slip borders[15]. With every successive iteration in VOF, the interface between two fluids is reconstructed using spatial information.

Advanced volume fraction expansion functions schemes,

such as piece-wise linear interface calculation (PLIC), coupled level set and volume of fluid (CLS-VOF) method, and simplified VOF (SVOF), were developed to overcome interface curvature challenges encountered when using the classic VOF scheme[10,16,17]. An interface capture approach based on a switching strategy had been developed by Darwish and Moukalled[18] with the Switching Technique for Advection and Capturing of Surfaces (STACS) scheme. Compressive advection interface capturing method (CAICM), a special VOF variant, has been applied to interface capturing of collapsing water columns by Pavlidis *et al*[19]. In order to develop bounded and accurate interface capture solutions, this computational methodology was developed using a high-order control volume finite element method (CVFEM) to obtain fluxes subject to flux-limiting (based on a normalised variable diagram) on control volume (CV) boundaries.

This research aims to investigate the impacts of temperature and core material composition on the flow dynamics during core relocation. The simulations were conducted using CAICM coupled with high-order accurate schemes discretised with streamline upwind Petrov-Galerkin (SUPG) method.

The remainder of this paper is structured as follows: Sections II and III describe the model formulation and validation, respectively, while Sections IV and V discuss core relocation and concluding remarks, respectively.

II. Model formulation

The model formulation in this study utilises higher-order CVFEM and CAICM with flux limiters using a normalised variable diagram approach.

The formulation is based on a family of unstructured triangles (2D) and tetrahedral (3D) element types, P_nDG-P_m and P_nDG-P_mDG[20]. Each finite element is split up into a number of CVs, which can be quadrilaterals (2D) or hexahedra (3D) as shown in Figure 1. For these element types, pressure is represented by a m^{th}-order polynomial in either continuous or discontinuous space, whereas velocity is represented by a n^{th}-order polynomial in discontinuous space. In this study, P_1DG-P_2 (Figure 1 linear discontinuous velocity function and quadratic continuous pressure function) elements were used for the model discretisation. In this formulation, scalars (such as temperature, density, volume fraction, etc.) are discretised in CV space, whereas pressure and velocity are discretised in FE space.

The model formulation is based on a multimaterial approach, in which the system is represented as a single phase made up of numerous immiscible materials (fluids) separated by distinct interfaces. This formulation models materials with discrete transported scalars (e.g., temperature, mass fraction) but with single velocity and pressure. Conservation equations were solved for the multimaterial components, but only the transport equation is shown here. Multimaterial formulations for continuity and momentum equations are fully described in[19,21,22]. In the absence of a source term, the advection-diffusion transport is expressed as,

$$\frac{\partial(\rho\alpha)}{\partial t} + \nabla\cdot(\rho\vec{u}\alpha) - \nabla\cdot\kappa\nabla\alpha = 0 \qquad (1)$$

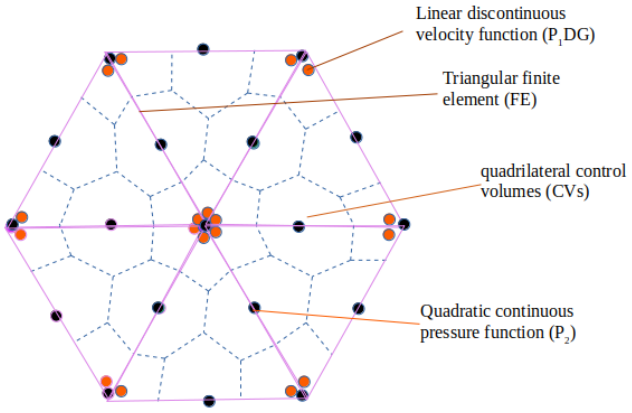

FIG. 1: Sketch of P_1DGP_2 element type. The tick pink line triangles are finite elements, quadrilateral dotted lines are control volumes, the black circles represent quadratic continuous pressure nodes, while the dimmed-red circles represent linear discontinuous velocity nodes.

where α is the transported scalar quantity (i.e., mass fraction, enthalpy (C_pdT)) and κ is the diffusion term. $\vec{u}$ is the flow velocity vector, ρ is the material density, C_p is the heat capacity, T is the temperature and t is time. Bulk thermophysical properties of the fluids can be expressed as:

$$\rho = \sum_{j=1}^{N}\alpha_j\rho_j;\ \kappa = \sum_{j=1}^{N}\alpha_j\kappa_j \text{ and } C_p = \sum_{j=1}^{N}\alpha_j C_{p,j}. \qquad (2)$$

where
α_j, ρ_j, κ_j and $C_{p,j}$ the mass fraction, density, diffusion term, and heat capacity, respectively of material j. $j = 1,2,\cdots N$, where N represents the total number of materials.

Discontinuities of flow fields across the fluid interfaces, complex topologies, and scale separation around CV surfaces are addressed using the Petrov-Galerkin spatial discretisation approach. A modified Crank-Nicolson scheme with a time-stepping parameter τ is used to discretise Eqn. 1 temporally and compute the advected quantity within the CV.

With the assumption of no source term in Eqn. 1, the transport equation is solved with the introduction of CV shape functions M_i. With Green's theorem, Eqn. 1 can be simplified using Petrov-Galerkin spatial discretisation approach and integration by parts to give Eqn. 3.

$$\int_{V_i} M_i\frac{\partial(\rho_j\alpha_j)}{\partial t} + \int_{V_i} M_i\rho_j\vec{u}\nabla\alpha_j - \int_{V_i}\kappa_j\cdot\nabla M_i\cdot\nabla\alpha_j = 0 \qquad (3)$$

The stiffness matrix from the third term of the integral in Eqn. 3 is symmetrical since α and M_i are exchangeable without any effects on the integral, whereas that of the second term is non-symmetrical. Eqn. 3 is further simplified to

$$\int_{V_i} M_i\frac{\partial(\rho_j\alpha_j)}{\partial t}dV + \int_{\partial V_i}(\vec{n}\cdot\vec{u}\rho_j\alpha_j - \vec{n}\cdot\kappa_j\nabla\rho_j\alpha_j)\,d\,\partial V_i \qquad (4)$$

∂V_i is the outward normal surface area of the control volume, and $i = 1,2,\cdots\mathscr{I}$, where $\mathscr{I}$ is the number of control volumes. n is the outward pointing unit vector to the surface (∂V_i)

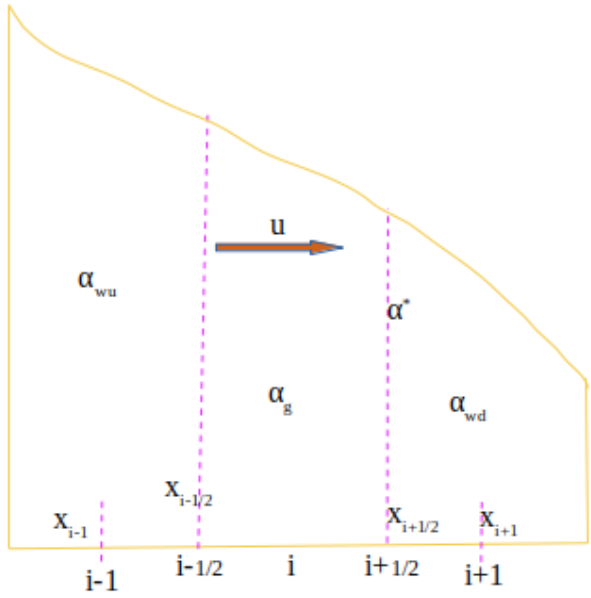

FIG. 2: 1D finite element diagram with downwind (*wd*), upwind (*wd*) and centered (*g*) CVs, with higher-order FE field reconstruction face value (α^*).

of the control volume. The difference between the advected and diffusive quantity within the FE space in the last term of Eqn. 4 gives the transported quantity, α^* across the interface as shown in Figure 2, represented in 1D. Introducing a time stepping parameter τ of value $1/2$, Eqn. 4 can be applied over each control volume, i as

$$\int_{V_i} M_i \left(\frac{\rho_{j,i}^{k+1}\alpha_{j,i}^{k+1} - \rho_{j,i}^{k}\alpha_{j,i}^{k}}{\Delta t} \right) dV$$
$$= \int_{\partial V_i} \tau_{j,i}^{k+\frac{1}{2}} \left(-u^{k+1}\rho_{j,i}^{k+1} \cdot n\alpha_{j,i}^{k+1} + n \cdot \kappa_{j,i}^{k+1} \nabla \alpha_{j,i}^{k+1} \right) d\,\partial V_i$$
$$+ \int_{\partial V_i} \left(1 - \tau_{j,i}^{k+\frac{1}{2}} \right) \left(-u^{k}\rho_{j,i}^{k} \cdot n\alpha_{j,i}^{k} + n \cdot \kappa_{j,i}^{k} \nabla \alpha_{j,i}^{k} \right) d\,\partial V_i \tag{5}$$

To compute the fluxes across the interface of node associated with CV i, extra nodes within CV, $i-\frac{1}{2}$ and $i+\frac{1}{2}$ were added between i and $i-1$, and i and $i+1$, respectively as shown in Figure 2. For a particular CV i with edge length of Δx ($x_i - x_{i+1}$), the advected quantity α across the interface of node between $i-\frac{1}{2}$ and $i+\frac{1}{2}$ at time-step k is set as $\alpha_{i+\frac{1}{2}}^{k}$ and $\alpha_{i-\frac{1}{2}}^{k}$, respectively as shown in Figure 2. The discretised form of Eqn. 1 becomes

$$\frac{\alpha_{j,i}^{k+1} - \alpha_{j,i}^{k}}{\Delta t} = \frac{1}{\Delta x_i} \left[\tau_{j,i-\frac{1}{2}}^{k+\frac{1}{2}} \left(n \cdot u_{i-\frac{1}{2}}^{k+1} \alpha_{j,i-\frac{1}{2}}^{k+1} - n \cdot \vartheta_{j,i-1/2}^{k+1} \nabla \alpha_{j,i-\frac{1}{2}}^{k+1} \right) + \left(1 - \tau_{j,i-\frac{1}{2}}^{k+\frac{1}{2}} \right) \left(n \cdot u_{i-\frac{1}{2}}^{k} \alpha_{j,i-\frac{1}{2}}^{k} - n \cdot \vartheta_{j,i-\frac{1}{2}}^{k} \nabla \alpha_{j,i-\frac{1}{2}}^{k} \right) - \tau_{j,i+\frac{1}{2}}^{k+\frac{1}{2}} \left(n \cdot u_{i+\frac{1}{2}}^{k+1} \alpha_{j,i+\frac{1}{2}}^{k+1} - n \cdot \vartheta_{j,i+1/2}^{k+1} \nabla \alpha_{j,i+\frac{1}{2}}^{k+1} \right) - \left(1 - \tau_{j,i+\frac{1}{2}}^{k+\frac{1}{2}} \right) \left(n \cdot u_{i-\frac{1}{2}}^{k} \alpha_{j,i-\frac{1}{2}}^{k} - n \cdot \vartheta_{j,i-\frac{1}{2}}^{k} \nabla \alpha_{j,i-\frac{1}{2}}^{k} \right) \right] \tag{6}$$

where $\left(n \cdot u_{i+\frac{1}{2}}^{k+1} \alpha_{j,i+\frac{1}{2}}^{k+1} - n \cdot \vartheta_{j,i+\frac{1}{2}}^{k+1} \nabla \alpha^{k+1}|_{j,i+\frac{1}{2}} \right) = q_{j,i+\frac{1}{2}}^{k+1}$ and $\left(n \cdot \vartheta_{j,i+1/2}^{k} \nabla \alpha^{k}|_{i+\frac{1}{2}} - n \cdot u_{i+\frac{1}{2}}^{k} \alpha_{j,i+\frac{1}{2}}^{k} \right) = -q_{j,i+\frac{1}{2}}^{k}$ are flux limiting values on the face $i+\frac{1}{2}$ at discrete times $k+1$ and k respectively. $\nabla \alpha^{k+1}|_{j,i+\frac{1}{2}}$ and $\nabla \alpha^{k}|_{j,i+\frac{1}{2}}$ are the gradient of the transported material at face $i+\frac{1}{2}$ for $k+1$ and k time-steps, respectively for material j. $\vartheta = \frac{\kappa}{\rho}$. The value of τ for face $i-\frac{1}{2}$ and face $i+\frac{1}{2}$ at time step from k to $k+1$ are given by $\tau_{j,i-\frac{1}{2}}^{k+\frac{1}{2}}$ and $\tau_{j,i+\frac{1}{2}}^{k+\frac{1}{2}}$, respectively. Equation 6 results in the transported quantities evaluated on the CV i at the time step $k+1$ relative to surrounding faces $i+\frac{1}{2}$ and $i-\frac{1}{2}$ as a function of their flux-limiting values. n can be expressed as the vector space normalisation in terms of the transported scalar gradient $\nabla\alpha$ $\left(n = \frac{\nabla \alpha}{|\nabla \alpha|} \right)$. Transported quantity is then given as

$$\alpha_{j,i}^{k+1} = \alpha_{j,i}^{k} + \frac{\Delta t}{\Delta x_i} \left[\tau_{j,i-\frac{1}{2}}^{k+1} q_{j,i-\frac{1}{2}}^{k+1} + \left(1 - \tau_{j,i-\frac{1}{2}}^{k+\frac{1}{2}} \right) q_{j,i-\frac{1}{2}}^{k} - \tau_{j,i+1/2}^{k+\frac{1}{2}} q_{j,i+\frac{1}{2}}^{k+1} - \left(1 - \tau_{j,i+1/2}^{k+1/2} \right) q_{j,i+\frac{1}{2}}^{k} \right] \tag{7}$$

The flux-limiting scheme was applied to the scalar's and flux transport across the interface of CV i connecting upwind and downwind CVs. Further details of the flux-limiter application with normalised variable diagram (NVD) approach are described in[19,23].

III. Model validation

For the validation of this model, the classical collapsing water column (CWC) was used based on experimental and simulation work by Cruchaga *et al*[24] and Yeoh and Barber[25], respectively. Cruchaga *et al*[24] designed an experiment with a water column height H to length L ratio of 2 (i.e., $A_r = 2$, $A_r = \frac{H}{L}$). The former[25], used the same water column height H to length L ratio (as used in this study, $A_r = 2$) for numerical interface capturing investigations using FVM-based ANSYS, Inc., CFX model. Water column of height H, was held with a barrier at one end (left side) of a tank. The time for the water column collapsing at different vertical and horizontal positions of the tank were recorded as the barrier was removed, which was simulated numerically. The laboratory experiment was performed such that the time evolution of the collapsing column was captured by a video camera and stopwatch install

on the tank. A qualitative validation is presented to compare the present study against the lab-scale and simulation experiments. The coupled CVFEM and CAICM model formulation was initially validated by Pavlidis *et al*[19] (simple advection and water collapsing column with multiphase flow model and anisotropic unstructured mesh), Xie *et al*[21] (falling liquid film, rising bubble, milkcrown phenomena with single phase and multi-component formulation) and Bregu *et al*[5] (water collapsing column, single/multi-phase and multi-component formulations).

The collapsing of the water column was under the influence of gravitational force. The physics behind collapsing water column and core relocation are the same. At 0.2 secs, the tank floor has almost been covered by the collapsed water in the three cases as seen in Figure 3. The water column collapsed under the influence of gravitational force. From Figure 3, it can be observed that the current study model is in good agreement with both studies.

FIG. 3: Model validation using cwc simulation experiments at 0.2 sec time for the present study (left), Yeoh and Barber[25] (center), and Cruchaga *et al*[24] (right).

TABLE I: Descriptions of the different scenarios of core relocation simulations

Descriptions	Considered scenarios	
	scenario 1	scenario 2
Core materials composition	UO_2 + air	(water, UO_2, graphite and zircaloy) + air
Core materials properties	individual material property	bulk materials properties
Percentage composition	100% UO_2 + air	[water (65%), UO_2 (10%), graphite (15%), zircaloy (10%)] + air

IV. Core relocation

When the reactor core is subjected to extreme thermal conditions, as explained in Section I, core materials can undergo melting. This melting occurs as a result of a change in the thermophysical properties of the materials. Investigating the behaviour of nuclear reactor cores under extreme conditions, such as severe accidents or core relocation is vital for the reactor safety improvement. Assessing the possibility and mechanisms of melted core materials relocating within the reactor vessel or containment structure during such events could help in maintaining reactor integrity. Exploring some factors such as heat flow, melted materials and structural components interactions, and potential consequences of such relocation on containment integrity are significant to nuclear safety improvement. Using models and simulations to predict the behaviour of melted materials during core relocation can ultimately inform safety measures, emergency response strategies, and reactor design improvements to mitigate severe accidents consequences.

In this study, the impact of corium composition on the flow dynamics during core relocation is numerically investigated. Simulations involving 2 case-scenarios were conducted as shown in Table I: The containment (including core material) in scenario 1 is comprised of UO_2 and air, while that of scenario 2 comprised of the combination of UO_2, zircaloy, graphite, water (of 10%, 10%, 15%, 65% composition, respectively) and air. Mesh resolution, mean flow velocity and temperature of the two scenarios are investigated. This is necessary to understand the response of different corium composition and impacts of temperature on the flow dynamics during core relocation. Figure 4 shows the initial unstructured mesh resolution and material configuration (at t = 0 s) for a grid-independent study. The domain is a 2D geometry of $L = 1\ m$ (see Figure 4) with 12050 triangular elements. Melted core materials are in the red-coloured region, while the rest of the domain is filled with air (in blue) at the onset of the core relocation. The corium collapse may be presented as symmetrical (as the corium is assumed w homogeneous thermophysical and rheological properties), however corium motion after it hits the bottom is not symmetrical. Here, we assume symmetry of the geometry and the next research stage will be a full 3D simulation (future work).

In the simulations presented here, core materials (UO_2, graphite, water and zircaloy) are assumed incompressible whereas air is assumed to behave according to the following equation of state.

$$\rho = \rho_\circ \left[1 + a\left(P - P_\circ\right) - b\left(T - T_\circ\right)\right] \tag{8}$$

where $\rho_\circ$ is the reference density, a and b are elasticity bulk modulus and thermal expansion coefficient given as 7.06×10^{-6} Pa^{-1} and 9.4×10^{-4} K^{-1}, respectively. P and T are pressure and temperature of the system, while $T_\circ$ and $P_\circ$ are the reference temperature (323 K) and pressure (1.0×10^5 Pa), respectively.

Temperature Dirichlet boundary condition of 1000 K is imposed on the walls of the reactor. Core materials were assumed to be fully melted (initially at a temperature of 2700 K) with the air temperature of 1200 K, and collapsed at the same time with no nuclear recriticality. The reactor coolant (water) was also assumed to exist in liquid form throughout the relocation event.

An anisotropic adaptive mesh method as described by Piggott *et al*[26] was used to optimally control mesh resolution based on the flow dynamics. Adaptive time steps with Courant-Friedrichs-Lewy (CFL) number of 5.0 were applied to simulations to capture sharp interfaces between core materials with good convergence. The method is able to dynamically focus mesh resolution at the interface between air and corium, whereas in the remaining domain, a coarse mesh can be used, reducing computational cost. A detailed description of the mesh adaptivity method used in this work can be found[27–29]. In the simulations shown in this Section, the mesh is adapted based on the UO_2 mass fraction with an interpola-

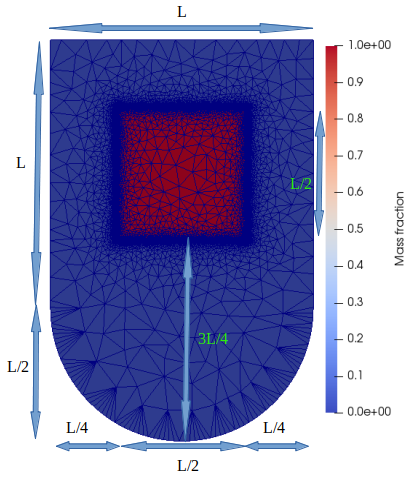

FIG. 4: Volume fraction representation of melted core with unstructured adaptive mesh. There are (initially) 12050 triangular P_1DG-P_2 elements.

tion error bound of 0.0005, a gradation parameter of 1.5, an aspect ratio bound of 3, and the mesh was adapted at every 3 time steps. Simulations were conducted using Intel Core i5 with 8 cores and 16GB RAM. Simulations of scenario 1 required 84 hours of wall clock time to complete. For scenario 2, simulations required 94.5 hours of wall clock time. This shows the higher computation cost of the bulk material simulation. Simulations for both case scenarios were initialised with mesh resolution of 12050 triangular P_1DGP_2 element-types.

Figure 6 shows time evolution of the number of CVs and elements for both cases (scenarios 1 and 2). Due to mesh resolution, the number of elements and CVs increase gradually at the early stage of the simulation. Mesh resolution follows similar pattern for both cases, though with larger number of elements used in scenario 2. There was a spike in number elements and CV evolution as the corium materials approach and hit the lower plenum (Figure 5). This shows slightly faster material relocation of scenario 1 than scenario 2 for the corresponding relocation time.

Figure 7 shows mean flow velocities for both case scenarios. There was an increase in the velocity at 0.70s as the corium hits the bottom of the plenum due to the splashing of the materials as shown in Figure 5. A larger spike in the mean velocity was observed for the simulation conducted for scenario 2. Simulations demonstrated that corium in scenario 1 reaches the lower plenum slightly faster than in scenario 2 with max mean velocity for both scenarios at 0.70s with a small (negligible) time-lag between them. This is expected as density (or weight) does not affect the time of free fall. Air resistance has limited/small impact on the speed of the fall.

The mean temperature over simulation time for both case scenarios are shown in Figure 8. Material 1 (UO_2 for scenario 1 and [water (65% w/w), UO_2 (10% w/w), graphite (15% w/w), zircaloy (10% w/w)] for scenario 2) was assumed to have melted, and mix with air while collapsing. A mean temperature fluctuation was observed during the relocation. Heat

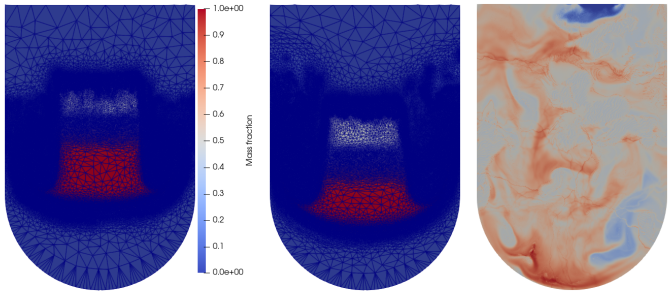

FIG. 5: Scenario 1 adaptive mesh at t=0.4s (left) and 0.99s, and mass fraction distribution at t=1.40s (right).

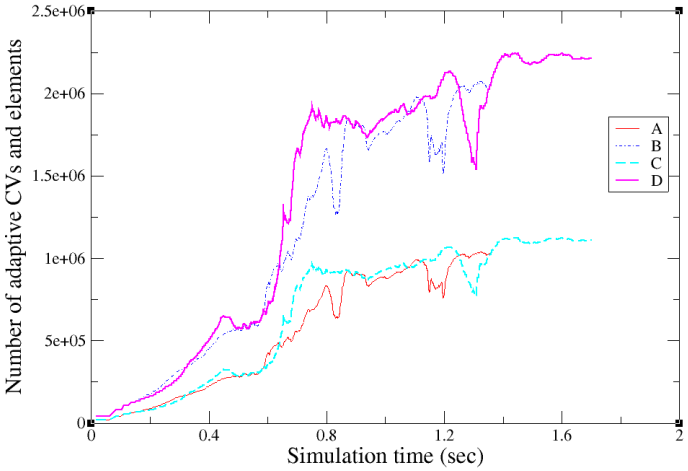

FIG. 6: Number of control volumes (CVs) and elements evolution. *A* and *B* represent number of elements and CVs for scenario 1, while *C* and *D* represent number of elements and CVs for scenario 2.

exchange between air and corium leads to mean temperature ranging from 1550K to 2265K. There was a higher temperature recorded for the bulk material case. This is attributed to the larger effective thermal conductivity in scenario 2 than in scenario 1 ($\kappa_{\text{eff}}^{\text{scenario 1}} = 6.80\text{W (m K)}^{-1}$ and $\kappa_{\text{eff}}^{\text{scenario 2}} = 23.424\text{W (m K)}^{-1}$, Table II).

V. Conclusion

In this study, impacts of temperature and core material composition on the flow dynamics during post-CHF events in PWRs are numerically investigated. Two corium material compositions (UO_2 and air for scenario 1 and [water (65% w/w), UO_2 (10% w/w), graphite (15% w/w), zircaloy (10% w/w)] and air for scenario 2) were considered to compare the impacts of temperature and their computation costs. The interface between corium materials is modelled through an integrated high-order accurate control volume finite element method (CVFEM) and the compressive advection interface capturing method (CAICM). To control numerical instabilities, the model was discretised using SUPG and the flux-limiting schemes with a normalised variable diagram ap-

TABLE II: Thermo-physical properties of air and corium materials at 2123 K and 100 bar[30,31]

Properties	Core materials percentage compositions				
Core materials	Water	UO_2	Zircaloy	Graphite	Air
Materials % composition (w/w)	65%	10%	10%	15%	
Density (kgm^{-3})	958.78	19100	6560	1710	1.2945 (reference density)
Specific heat capacity ($J(kg\ K)^{-1}$)	4184	280	285	720	1006
Thermal conductivity ($W(m\ K)^{-1}$)	0.591	6.80	13.6	140	0.025
Viscosity ($kg(m\ s)^{-1}$)	2.822×10^{-4}	6.5	10.3	10	2.181×10^{-5}

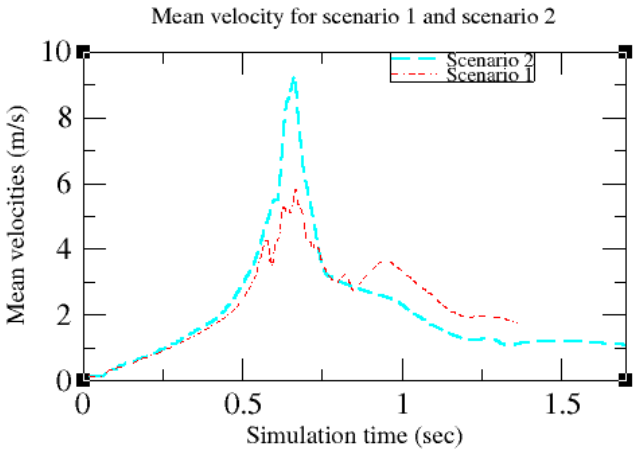

FIG. 7: Mean flow velocity for scenarios 1 (individual) and 2 (bulk).

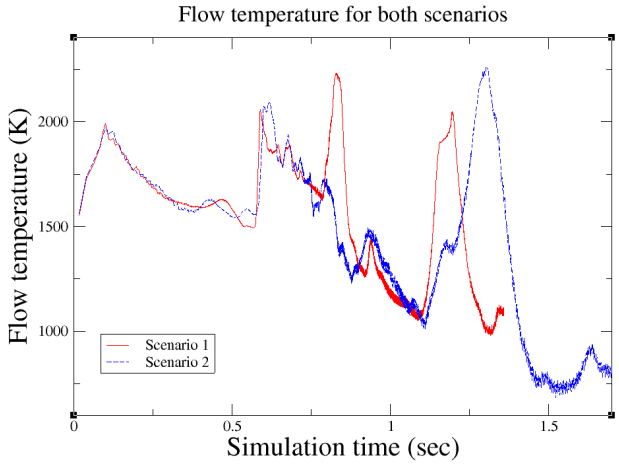

FIG. 8: Corium and air mean temperature for both cases.

proach. Mesh adaptivity algorithm was applied to focus resolution at the corium-air interfaces. Using EoS for the gas phase, the effects of air density variation on the corium mass fraction transport were determined. From the results of this study, the following conclusions are made:

- Air compressibility has a greater impact on the transport of scenario 2 corium than that of scenario 1 during core relocation events.
- Splashing of the corium after hitting the bottom of the plenum resulted in mean flow velocity increase and temperature fluctuation.
- Simulated mean corium temperature and velocity have similar orders of magnitude for both scenarios.

In summary, based on the results presented in Section IV, fluid and thermal energy flow dynamics (mean flow velocity and temperature) are similar for scenarios 1 (ie lumping all materials into UO_2) and 2 (explicitly defining properties of all corium materials). However, computational cost for simulating scenario 1 is significantly smaller than for scenario 2 (84h and 94.5h of wall-time processed in an Intel Core i5 with 8 cores and 16GB RAM). Multiphase interface capturing requires high mesh resolution and computational cost. Mesh adaptivity is used to focus grid resolution at the relevant physics, in this case the interface between all materials of the corium, to minimise computational cost without compromising numerical accuracy. As a good CFD practice, we start simulations with mesh-grids that is deemed as grid-independent. Pain *et al*[32], Hiester *et al*[29], Adam *et al*[28] and Xu *et al*[27] described how finite elements' shapes and topology change according to flow criteria to ensure numerical stability and convergence with controlled impact on numerical accuracy. Future work will extend the model to simulate core relocation in 3D.

Acknowledgments

The first author wishes to thank the Petroleum Trust Development Fund (PTDF), Nigeria for providing the funding for this research with grant number PTDF/ED/OSS/PHD/SAA/1801/20-20PHD109.

Data Availability Statement

The authors of this manuscript give their consent for the information in this manuscript to be published and made for public use for research and learning purposes. We understand that the text and any pictures published in the article will be freely available on the internet and may be seen by the general public. The pictures and text may also appear on other websites or in print, may be translated into other languages or used for commercial purposes.

[1]H. Madokoro and I. Sato, "Estimation of the core degradation and relocation at the Fukushima Daiichi Nuclear Power Station Unit 2 based on RE-

LAP/SCDAPSIM analysis," Nuclear Engineering and Design **376**, 111123 (2021).

[2]S. J. Hong, D. K. Ko, G. H. Lee, Y. A. Kim, K. S. Park, H. W. Kim, C. G. Kim, and G. H. Jang, "An assessment of radiation exposure of workers during decommissioning of reactor vessel at Kori unit 1," Nuclear Engineering and Design **392**, 111771 (2022).

[3]N. Zhao, Y. Chen, W. Ma, S. Bechta, and P. Isaksson, "A nodal sensitivity study of MELCOR simulation for severe accidents in a pressurized water reactor," Annals of Nuclear Energy **160**, 108373 (2021).

[4]S. H. Gyepi-Garbrah and T. Nitheanandan, "Severe accident prevention and mitigation in pressurized heavy water reactors," in *Pressurized Heavy Water Reactors* (INC, 2022) pp. 477–508.

[5]E. Bregu, S. A. Ajah, and J. Gomes, https://doi.org/10.14295/vetor.v33i2.15158, journal = VETOR - Revista De Ciências Exatas E Engenharias, number = 2, pages = 2–10, title = Nuclear Meltdown Relocation and Core Catcher Analysis, url = https://doi.org/10.14295/vetor.v33i2.15158, volume = 33, year = 2023.

[6]T. B. Nguyen, D. Liu, M. I. Kayes, B. Wang, N. Rashin, P. W. Leu, and T. Tran, "Critical heat flux enhancement in pool boiling through increased rewetting on nanopillar array surfaces," Scientific Reports **8**, 1–9 (2018).

[7]P. Fernández-Arias, D. Vergara, and J. A. Orosa, "A global review of PWR nuclear power plants," Applied Sciences **10**, 1–28 (2020).

[8]J. Wang, C. Wang, K. Shi, and G. Su, "Review on core degradation and material migration research in light-water reactors," Frontiers in Energy Research **6**, 1–10 (2018).

[9]D. Zhan, X. Zhao, S. Xia, P. Chen, and H. Chen, "Numerical Simulation and Validation for Early Core Degradation Phase under Severe Accidents," Science and Technology of Nuclear Installations **2020** (2020), 10.1155/2020/6798738.

[10]B. M. Ningegowda and B. Premachandran, "A Coupled Level Set and Volume of Fluid method with multi-directional advection algorithms for two-phase flows with and without phase change," International Journal of Heat and Mass Transfer **79**, 532–550 (2014).

[11]S. McKee, M. F. Tomé, V. G. Ferreira, J. A. Cuminato, A. Castelo, F. S. Sousa, and N. Mangiavacchi, "The MAC method," Computers and Fluids **37**, 907–930 (2008).

[12]S. Noro, H. Koibuchi, S. Hongo, S. Nagahiro, H. Ikai, M. Nakayama, T. Uchimoto, and J.-P. Rieu, "Langevin Navier-Stokes simulation of protoplasmic streaming by 2D MAC method," arXiv preprint arXiv:2112.10901 , 1–17 (2021), arXiv:2112.10901.

[13]S. Shin, J. Chergui, D. Juric, L. Kahouadji, O. K. Matar, R. V. Craster, S. Shin, J. Chergui, D. Juric, L. Kahouadji, and O. K. Matar, "An Interface-tracking Technique for Multiphase Flow with Soluble Surfacant," Journal of Computational Physics **359**, 409–435 (2018).

[14]Z. Huang, G. Lin, and A. M. Ardekani, "A consistent and conservative Phase-Field model for thermo-gas-liquid-solid flows including liquid-solid phase change," Journal of Computational Physics **449**, 110795 (2022), arXiv:2102.06863.

[15]D. A. Hoang, V. van Steijn, L. M. Portela, M. T. Kreutzer, and C. R. Kleijn, "Benchmark numerical simulations of segmented two-phase flows in microchannels using the Volume of Fluid method," Computers and Fluids **86**, 28–36 (2013).

[16]I. Chakraborty, G. Biswas, and P. S. Ghoshdastidar, "A coupled level-set and volume-of-fluid method for the buoyant rise of gas bubbles in liquids," International Journal of Heat and Mass Transfer **58**, 240–259 (2013).

[17]F. Xiao, S. Ii, and C. Chen, "Revisit to the THINC scheme: A simple algebraic VOF algorithm," Journal of Computational Physics **230**, 7086–7092 (2011).

[18]M. Darwish and F. Moukalled, "Convective Schemes for Capturing Interfaces of Free-Surface Flows on Unstructured Grids," Numerical Heat Transfer, Part B **49**, 19–42 (2006).

[19]D. Pavlidis, J. L. M. A. Gomes, Z. Xie, J. R. Percival, C. C. Pain, and O. K. Matar, "Compressive advection and multi-component methods for interface-capturing," International Journal for Numerical Methods in Fluids **80**, 256–282 (2016).

[20]P. Salinas, J. R. Percival, D. Pavlidis, Z. Xie, J. Gomes, C. C. Pain, and M. D. Jackson, "A discontinuous overlapping control volume finite element method for multi-phase porous media flow using dynamic unstructured mesh optimization," Society of Petroleum Engineers - SPE Reservoir Simulation Symposium 2015 **3**, 1511–1528 (2015).

[21]Z. Xie, D. Pavlidis, P. Salinas, J. R. Percival, C. C. Pain, and O. K. Matar, "A balanced-force control volume finite element method for interfacial flows with surface tension using adaptive anisotropic unstructured meshes," Computers and Fluids **138**, 38–50 (2016).

[22]H. Lee and S. H. Rhee, "A dynamic interface compression method for VOF simulations," Journal of Mechanical Science and Technology **29**, 1849–1857 (2015).

[23]M. Darwish and F. Moukalled, "The χ Schemes : A New Consistent High-Resolution Formulation Based on the Normalized Variable Methodology," Tech. Rep. (2020).

[24]M. A. Cruchaga, D. J. Celentano, and T. E. Tezduyar, "Collapse of a liquid column: Numerical simulation and experimental validation," Computational Mechanics **39**, 453–476 (2007).

[25]G. H. Yeoh and T. Barber, "Assessment of interface capturing methods in Computational Fluid Dynamics (CFD) codes - A case study," Journal of Computational Multiphase Flows **1**, 201–215 (2009).

[26]M. D. Piggott, P. E. Farrell, C. R. Wilson, G. J. Gorman, and C. C. Pain, "Anisotropic mesh adaptivity for multi-scale ocean modelling," Philosophical Transactions of the Royal Society A: Mathematical, Physical and Engineering Sciences **367**, 4591–4611 (2009).

[27]X. Xu, C. C. Pain, A. J. Goddard, and C. R. De Oliveira, "An automatic adaptive meshing technique for Delaunay triangulations," Computer Methods in Applied Mechanics and Engineering **161**, 297–303 (1998).

[28]A. Adam, D. Pavlidis, J. R. Percival, P. Salinas, Z. Xie, F. Fang, C. C. Pain, A. H. Muggeridge, and M. D. Jackson, "Higher-order conservative interpolation between control-volume meshes: Application to advection and multiphase flow problems with dynamic mesh adaptivity," Journal of Computational Physics **321**, 512–531 (2016).

[29]H. R. Hiester, M. D. Piggott, P. E. Farrell, and P. A. Allison, "Assessment of spurious mixing in adaptive mesh simulations of the two-dimensional lock-exchange," Ocean Modelling **73**, 30–44 (2014).

[30]L. Ma, J. Wang, A. M. Marconnet, A. C. Barbati, G. H. McKinley, W. Liu, and G. Chen, "Viscosity and thermal conductivity of stable graphite suspensions near percolation," Nano Letters **15**, 127–133 (2015).

[31]T. Kondo, H. Muta, K. Kurosaki, F. Kargl, A. Yamaji, M. Furuya, and O. Y, "Density and viscosity of liquid ZrO2 measured by aerodynamic levitation technique," Heliyon **5**, 1–7 (2019).

[32]C. C. Pain, A. P. Umpleby, C. R. de Oliveira, and A. J. Goddard, "Tetrahedral mesh optimisation and adaptivity for steady-state and transient finite element calculations," Computer Methods in Applied Mechanics and Engineering **190**, 3771–3796 (2001).